Extended SZ map of the most luminous X-ray cluster, RXJ1347-1145

E. Pointecouteau, M. Giard
Centre d'Etude Spatiale des Rayonnements
9 av du colonel Roche, BP4346, F-31028 Toulouse cedex 4, France
pointeco@cesr.fr

A. Benoit
Centre de Recherche des Très Basses Températures
25 avenue des Martyrs, BP 166 , F-38042, Grenoble Cedex 9, France

F.X. Désert
Laboratoire d'Astrophysique de l'Observatoire de Grenoble
414 rue de la piscine, F-38041 Grenoble Cedex 9, France

J.P. Bernard, N. Coron, J.M. Lamarre
Institut d'Astrophysique Spatiale
Bât 121, Université Paris-Sud, F-91405 Orsay cedex, France

ABSTRACT

We present in this letter a high resolution (22" FWHM) extended map at 2.1mm of the Sunyaev-Zel'dovich effect toward the most luminous X-ray cluster, RXJ1347-1145. These observations have been performed with the DIABOLO photometer working at the focus of the 30m IRAM radiotelescope. We have derived a projected gas mass of $(1.1 \pm 0.1) \times 10^{14}\, h_{50}^{-5/2} \mathrm{M}_{\odot}$ within an angular radius of $\theta = 74''$ (ie: projected radius of 0.6Mpc, H_0 = 50km/s/Mpc, $\Omega_m = 0.3$, $\Omega_\Lambda = 0.7$). This result matches very well the expected gas mass from the cluster models of X-ray data. With an unprecedented sensitivity level our measurement does not show significant departure from a spherical distribution. The data analysis also allows us to characterize the 2.1mm flux of a well known radio source lying in the center of the cluster: $F_{RS}(2.1\mathrm{mm}) = 5.7 \pm 1.6$mJy.

Subject headings: cosmology: cosmic microwave background — cosmology: observations — galaxies: clusters: individual (RXJ1347-1145) — intergalactic medium

1. Introduction

The statistical properties of galaxy clusters (shape, structures, size, temperature, mass) depend strongly on the geometry of the Universe. Their study provides some robust constraints on cosmological models, structure formations and evolution (Oukbir, Bartlett and Blanchard 1997; Sadat, Blanchard and Oukbir 1998; Bahcall and Fan 1998). This strong coupling makes the study of massive and distant clusters a very useful tool for cosmology. The intergalactic gas component can be observed through its Bremsstrahlung emission at X-ray wavelengths. It can also be detected from submillimeter to radio wavelengths via the Sunyaev-Zel'dovich effect (Sunyaev and Zel'dovich 1972). Whereas the X-ray emission depends on the square of the gas density, the Sunyaev-Zel'dovich (SZ hereafter) effect is linearly dependent on this quantity. For this reason, the SZ effect is proportional to the column density and thus to the line of sight integrated gas mass. Moreover the SZ signal does not suffer from the brightness decrease of the radiations (in particular the X-ray one) due to the expansion of the Universe (see a review by Birkinshaw (1999)).

The RXJ1347-1145 cluster is known as the most luminous X-ray cluster to date. It has been detected in the ROSAT All Sky Survey and furthermore studied with the ROSAT-HRI and the ASCA-GIS2 instruments (Schindler et al. 1995, 1997). With an intrinsic bolometric X-ray luminosity of $L_{bol} = 21 \times 10^{45}\, h_{50}^{-2}$ergs s^{-1}, it shows a very peaked X-ray emission profile with an angular core radius of $\theta_c = 8.4 \pm 1.8$". It also presents a very strong cooling flow in its central region, with a corresponding accreting rate of $\dot{\mathrm{M}}_{cool} = 3000\mathrm{M}_\odot$/yr. It is a distant cluster with $z = 0.45$, so that the angular distance is $1670\, h_{50}^{-1}$Mpc (490pc/arcmin, with $H_0 = 50$km/s/Mpc, $\Omega_m = 0.3$, $\Omega_\Lambda = 0.7$; 410pc/arcmin in a standard CDM model). The value of the core radius with these two sets of cosmological parameters is respectively equal to 68kpc (ΛCMD model) and to 57kpc (standard CDM model). The total binding mass derived from the X-ray data within 1Mpc is $M_{tot} = 5.8 \times 10^{14}\, h_{50}^{-1}\mathrm{M}_\odot$. This value has to be compared to those obtained from the optical gravitational lensing follow-up achieved by Fischer and Tyson (1997) and Sahu et al. (1998). Within the same radius, they provide a value of $M_{tot} = 1.7 \times 10^{15}\, h_{50}^{-1}\mathrm{M}_\odot$ (Fischer and Tyson 1997).

In a previous paper, we have reported the detection of a very strong SZ effect in the direction of RXJ1347-1145 with the DIABOLO photometer (Pointecouteau et al. 1999). We have presented a map of the cluster central region ($2' \times 1'$). The corresponding Comptonization parameter was $y(0) = 12.7^{+2.9}_{-3.1} \times 10^{-4}$ (1σ error bars). During the 1999 DIABOLO run, we performed an extended mapping of RXJ1347-1145 over a 4' by 4' field. The size of the first map was rather small so that only 1D average slice was used to compare with the X-ray data. Here the size of the map allows to make full use of 2D information on the cluster. Moreover, the computation of a cluster radial profile from a 2D map allows to discard most of the effects induced by point sources.

In this paper, we present the resulting extended map of this cluster at 2.1mm. In a first part, we detail the observations procedures and characteristics (see Sec 2). In a second time (see Sec 3), we describe the data processing. In section 4, we analyze the astrophysical data. In the last part (see Sec 5), we discuss the results. Throughout this paper, we will use the following values for the cosmological parameters: $H_0 = 50$km/s/Mpc, $\Omega_m = 0.3$, $\Omega_\Lambda = 0.7$.

2. Observations

The DIABOLO instrument is a dual channel photometer working at 1.2 and 2.1mm. The detectors are bolometers cooled down to 0.1K using an open cycle ^{4}He-^{3}He dilution refrigerator (Benoit et al. 2000). Two thermometers associated to a heater and a PID digital control system are used to regulate the temperature of the 0.1K plate. There are three adjacent bolometers per channel, arranged in an equilateral triangle at the focus of the telescope. For a given channel, each bolometer is coaligned with one bolometer of the second channel, both looking toward the same sky direction. For the observations presented here, DIABOLO was installed at the focus of the IRAM 30 meter radio telescope at Pico Veleta (Spain). This configuration allows us to achieve a 22" resolution at 2.1mm. The 30 meter telescope focus being of Nasmyth type, the rotation of the field has to be taken into account in the sky maps reconstruction. Désert et al. (1998) have described the experimental setup and reported the first DIABOLO SZ detections.

RXJ1347-1145 has been observed in January 1999 for a total integration time of 17 hours. The X-ray emission center: $\alpha_{2000} = 13^{\mathrm{h}}47^{\mathrm{m}}31^{\mathrm{s}}$, $\delta_{2000} = -11°45'11$" (Schindler et al. 1997), has been taken as the map center. Each sequence of observation has been performed in the right ascension coordinates, using the Earth rotation as right ascension drift such that the telescope is kept fixed in local coordinates. The basic observation sequence was a $240'' \times 240''$ map in right ascension-declination coordinates, with a 10" declination steps. The wobbling secondary mirror of the 30m IRAM telescope has been used at a frequency of 1Hz and with a modulation amplitude of 150". The wobbling is horizontal (eg: at constant elevation), thus not aligned with the scanning direction. In order to remove systematic signal drifts that are produced by the antenna environment, we used alternatively the positive and negative beam to map the cluster. We have produced 89 such maps.

3. Data reduction and calibration

The data processing includes all the different steps described by Pointecouteau et al. (1999). This includes a correction from the cosmic-rays impacts, a synchronous demodulation of the signal, a subtraction of the atmospheric signal correlated between the two channels, a correction from the atmosphere opacity, a reprojection of each single observation on a final RA-DEC grid, a baseline subtraction supported by the edges of the map and the computation of a final map at 1.2 and 2.1mm by coadding the 3 bolometers of each channel. The beam modulation is performed with an amplitude of 150", so that some of the "OFF" positions lie within the limit of our map. Consequently, the beam switching has to be taken into account in the data analysis (see Sec. 4.1).

Throughout the run, the pointing verifications have been performed in the direction of QSOs lying at about the same declination as the cluster. The planet Mars has been used as a calibration target and to map the beam pattern. Assuming Mars is a point source with respect to the DIABOLO's beam (angular diameter around 5" in January 1999), the accuracy in the absolute calibration is better than 20% at 1.2mm and 15% at 2.1mm. Mars has directly been mapped in right ascension-declination during this run. This method provides a direct view of the beam shape including eventual systematic effect as the beam elongation in the right-ascension direction due to the conjugated effects of the scanning drift speed and the bolometer time constant.

4. Results and data analysis

The reduced map for RXJ1347-1145 at 2.1mm is shown on Fig. 1a. It has been smoothed using a Gaussian filter with 20" FWHM. The contours overplotted correspond to 1, 2, 3, 4 and 5 σ detection levels (negative and positive contours are respectively drawn with solid and dashed lines). The noise level on this map is 1mJy/beam in a $10'' \times 10''$ pixel (equivalent to 0.5mJy/beam in the 22" DIABOLO beam and to 0.3mJy/beam (equivalent to $y = 3 \times 10^{-5}$) in the 30" FWHM effective beam after smoothing). This map exhibits a strong and extended SZ decrement in the direction of the cluster. Unfortunately, the DIABOLO 1.2mm data are very noisy. No positive SZ signal could be extract from them. We used them to subtract most of the atmospheric emission from the 2.1mm data.

The signal does not seem to follow a symmetric circular distribution as expected from the X-ray data and from the commonly used β-model. The first look at the map argues in favor of substructure in the signal, and so far, in the gas distribution. The X-ray map has been overplotted on the SZ map (see Fig. 1c). It has been computed from the whole ROSAT/HRI observations (35ks exposure time) obtained from the ROSAT database (the map published by Schindler et al. (1997) included only a third of those data).

As the SZ signal is linearly dependent of the gas density (scaled with n_e), the X-ray emission is dominated by contributions from regions of higher density (scaled with n_e^2). Furthermore, the X-ray and SZ signals are not sensitive to the same part of the gas. What appears as differences between the SZ and the X-ray spatial distributions could be associated to different gas phases with various physical states (density, pressure, temperature). In the following, we will compare in detail the measured SZ map to the expected SZ distribution deduced from the symmetrical cluster X-ray model.

4.1. Modeling the SZ signal

From the ROSAT-HRI X-ray map and the ASCA X-ray spectrum of RXJ1347-1145 Schindler et al. (1995, 1997) have extracted the cluster physical parameters: $T_e = 9.3 \pm 0.5$keV, $n_{e0} = 9.4 \times 10^{-3}$cm^{-3}, $\theta_c = 8.4 \pm 1.8$" and $\beta = 0.56 \pm 0.04$ (1σ errors), assuming a β-model for the gas distribution (Cavaliere and Fusco-Femiano 1976). Using those parameters, we can compute the Comptonization parameter expected toward the cluster center: $y_{exp}(0) = (8.4 \pm 2.7) \times 10^{-4}\, h_{50}^{1/2}$. Following this approach, we used a β-model to describe our SZ signal. Because of the circular symmetry induced on the projected sky by this kind of model, we chose to test different β-models on the radial profile resulting from our 2.1mm map (see Fig. 2). To model the SZ signal, we have taken into account the integration of the SZ spectrum on the DIABOLO passbands and the integration of the gas distribution over the DIABOLO beam shape. To perform a rigorous fit of the DIABOLO data, we need to take into account in the model every step of the observing procedure and of the data reduction procedure . So whatever the model we used, we considered it as a real sky and we reproduced on it all the DIABOLO's observations performed in the direction of RXJ1347-1147. (This includes the wobbling positions and amplitudes.). The resulting simulated data set of observations has been reduced in the same way as the real dataset by following all steps of the DIABOLO pipeline (demodulation, base line subtraction, reprojection,... see Sec 3).

The resulting model for the flux of the SZ decrement per beam can be expressed as follow:

$$F(\bar{\nu}, \overrightarrow{\Omega}) = y(0) \int \tau\nu SZ(\nu, T_g) d\nu \int P(\overrightarrow{\Omega}) L(\overrightarrow{\Omega} - \overrightarrow{\Omega'}) d\overrightarrow{\Omega'} \qquad (1)$$

where $y(0) = (k_B T_g / m_e c^2) \sigma_T \int n_e(l) dl$, is the Comptonization parameter towards the cluster center (k_B is the Boltzmann constant, m_e the electron mass and c the speed of light. σ_T is the Thomson cross section, $n_e(l)$ is the electronic density along the line of sight). $\tau(\nu)$ is the normalized DIABOLO band spectral efficiency. $SZ(\nu, T_g)$ represents the SZ spectrum. It is a numerical function of ν and T_g with a weak dependence on T_g that takes into account the relativistic corrections (Pointecouteau, Giard and Barret 1998). $P(\overrightarrow{\Omega})$ represents the normalized gas profile projected on the sky and $L(\overrightarrow{\Omega})$ is the normalized DIABOLO beam shape.

The cluster central region contains a radio point source, known from the NRAO VLA Sky Survey (NVSS) (Condon et al. 1998), which coordinates are α_{2000} =$13^h 47^m 30.7^s$ and δ_{2000} =-$11^\circ 45^m 8.6^s$ (within the 3" of the X-ray center). To avoid any contamination and bias of the SZ signal due to a residual millimeter emission of this radio point source, we chose to include its contribution in our model. We considered this source as a point source with respect to the DIABOLO's beam. This approach follows the method used by Pointecouteau et al. (1999):

$$F(\bar{\nu}, \overrightarrow{\Omega}) = F_{RS}(\bar{\nu}) L(\overrightarrow{\Omega}) \qquad (2)$$

$F_{RS}(\bar{\nu})$ is the flux of the point source.

We have tested a total of five models on our data. The models A and B just include an SZ component. In model A, we choose the Comptonization parameter, the core radius and β as free parameters. In model B, we just let free y and r_c and fixed β to 0.56 (the X-ray value). The three other models are a combination of an SZ component and a point source component. The parameters in model C are y, r_c, β and F_{RS}. In model D, we let free the y, r_c and F_{RS} parameters (β = 0.56). Finally, for the E model, we have fixed the core radius and the β parameters to their respective X-ray value of 8.4" and 0.56. We used the y and F_{RS} as free parameters. The models have been tested using a maximum likelihood analysis method. The errors are obtained through the integration of the likelyhood function over the parameter space. The best fit parameters are gathered for the different cases in table 1.

As shown by the results from models A and C, we can not constraint the core radius and the β parameters simultaneously, because those two parameters are too strongly coupled. For this reason β has been fixed to the X-ray value of 0.56 in models B and D. Unfortunately, in those two cases the core radius can also not be constraint precisely. Its determination suffers from a degeneracy and despite of the extent of our SZ map, we are not able to discriminate between a small and a high core radius model. This is due to the way we have defined the zero level: a baseline subtraction in the RA direction fitted to 60% of the data point per line 30% on each edge). This operation is needed to eliminate the low-frequency detector noises. Consequently, whatever the model is, the cluster extension is cut off by the baseline subtraction and the signal to noise ratio does not allow to make the difference between small and large core radius. For this reason, we have chosen to use the core radius value derived from the X-ray analysis, θ_c = 8.4", to describe the spatial gas distribution with a β-model. Following this hypothesis, we have adopted the model E as the best fit model. The best fit parameters are $y(0) = (7.9 \pm 0.5) \times 10^{-4}$ and $F_{RS} = 5.7 \pm 1.6$mJy (with 68% confidence level error bars). In order to perform an accurate error analysis, we have also propagated the uncertainty on the X-ray parameter determination through the whole pipeline of the data analysis. The extra 1σ errors are $\Delta y = 1.1 \times 10^{-4}$ and $\Delta F_{RS} = 1.8$mJy. Because we just use the information on the X-ray temperature to fix the exact shape of the SZ spectra (a second order effect), the extra errors induced by the temperature uncertainty is marginally significant. The most important difference is driven by the core radius and by the β parameters uncertainties. Figure 2 presents the best fit radial profile model (SZ plus point source signals) overlying the cluster radial profile as seen by DIABOLO at 2.1mm. The residual signal is overplotted as a dashed line.

One can also perform a fit with y as a single free parameter. To do that, the central part of the map ($\theta_c < 30$") is excluded from the radial profile computation. The best fit parameter in this case is $y(0) = (7.8 \pm 0.4) \times 10^{-4}$. Afterward, the point source flux can be derived from the residual map: $F_{RS} = 5.3 \pm 1.0$mJy. Those two values are fully consistent with the previous ones. (The propagation of the X-ray parameters uncertainties reach to respective extra errors of $\Delta y = 1.0 \times 10^{-4}$ and $\Delta F_\nu = 1.2$mJy). Our y value is in very good agreement within a 68% confidence level with the value expected from X-ray data. Moreover, it is in very good agreement with the value determined by Komatsu et al. (2000) from their 21GHz data: $y(0) = (7.7 \pm 1.6) \times 10^{-4}$. Finally, within the 2σ of our previous determination: $y(0) = 12.7^{+2.9}_{-3.1} \times 10^{-4}$ (Pointecouteau et al. 1999). Combining the $y(0)$ value expected from the X-ray data ($y_{exp}(0) = (8.4 \pm 2.7) \times 10^{-4}\, h_{50}^{1/2}$) and the one we estimated from our SZ measurements, we are able to derived the H_0 value: $H_0 = 44 \pm 6$km/s/Mpc. The error quoted on H_0 just includes the uncertainty on our $y(0)$ determination. If the uncertainties on the X-ray parameters are taken into account, the error on H_0 become ± 15km/s/Mpc. Obviously this does not take into account any other uncertainty or any systematic errors due to the cluster geometry or to the hypothesis concerning the gas isothermality or the hydrostatic equilibrium.

The residual signal resulting from the data map and the best fit model map difference is presented on figure 1b (A Gaussian 20" FWHM filtering has been performed). The 1, 2 and 3 σ detection levels have been overplotted (solid contours for the negative signal). This map is mostly compatible with noise, the higher deviation being a decrement (-3.1 ± 0.9mJy) located to the North-East of the cluster center ($\Delta\alpha = +35''$,$\Delta\delta = +30''$), with a significance: 3.5σ.

Komatsu et al. (2000) have mapped RXJ1347-1145 at at 150GHz with the NOBA/NRO instrument. They get a $2' \times 2'$ map of the cluster center. To compare our work to theirs, we have divided the center of our map in the same 4 regions ($50'' \times 50''$ square), SE, NE, NW and SW, as they did. We have integrated the flux in each region. The value derived for each region can then be compared to the one extracted from the NOBA/NRO map. The results are gathered in table 2. We also show the integrated values for our residual map. We do not confirm the negative excess for the SE quadrant. Instead, our measurement is symmetrical within the noise level. If any departure is to be searched in our map, then it is a positive excess in the SW quadrant: 2.8 ± 1.4. Despite the low significance level of this excess and refering to our residual map, we can suggest that this excess is compatible with the presence of a second point source in this region. This hypothesis is supported by the point source detected at 350GHz with SCUBA and at 8.46GHz with the VLA by Komatsu et al (private communication). Its VLA position is α_{2000}=$13^h47^m27.72^s$, δ_{2000}=-$11°45^m52.86^s$. The SCUBA and VLA respective fluxes are 17.9 ± 4.8mJy and 0.490 ± 0.043mJy. This source seems to be an infrared source. A millimeter residual, provided by the millimeter tail of a dust emission, could contribute to our signal. Complementary millimeter observations are needed for this source.

4.2. The gas mass profile

From the DIABOLO map, we can directly estimate the gas mass which gives rise to the measured SZ signal. The SZ signal can directly converted into a gas mass value by applying the linear transformation: $M(\theta) = C \times F_\nu(\theta)$, where C is a constant which depends on the redshift ($z = 0.45$) and also on the gas temperature. The SZ signal map is obtained after the subtraction of the point source best fit model (see Sec. 4.1). This RXJ1347-1145 SZ map is shown on figure 1c (The X-ray contours have been overplotted). Afterwards, it is converted into a gas mass map, which is then integrated with respect to the distance to the cluster center (see Fig. 3).

Due to the size of the DIABOLO map and especially to the part used to subtract the baseline (30% on the edge of each line), we could only measure the projected gas mass within a projected radius of 74" (ie: 0.6Mpc): $M_{gas}^{SZ}(\theta < 74'') = (1.1 \pm 0.1) \times 10^{14}\, h_{50}^{-5/2} \mathrm{M}_{\odot}$. The error bar are quoted at a 68% confidence level. This value agrees very well with the estimate gas mass derived from the X-ray best fit model (under the hypothesis of a spherical β-model): $M_{gas}^{\beta-model}(r < 0.6\mathrm{Mpc}) = 10^{14}\, h^{-5/2} \mathrm{M}_{\odot}$.

This result confirms the agreement of the SZ and the X-ray data, when the hypothesis of the β-model is adopted. In our case, no bias has been introduced in the measured projected mass by the baseline subtraction. In fact the part of each line used to subtract the baseline has been taken out of 0.6Mpc from the cluster center. A radius of 0.6Mpc corresponds to an angular radius of 74.2" ($8.8 r_c$). Assuming a virial radius of $10 r_c$, the mass unaccounted for is estimated as no more than 16% of the total gas mass.

Our determination of the gas mass agrees with the X-ray determination. However, the X-ray total mass determination disagree with the strong lensing (Sahu et al. 1998) and the weak lensing (Fischer and Tyson 1997) determinations by a factor of two. Allen (1998) explained this discrepancy by the effect of the cooling flow on the total mass estimation through X-ray data. He concludes that the correction from this effect removes the differences between the estimators of the total mass. As an example, we can propose an increase of the gas temperature by a factor of two ($\sim$ 18keV). To keep the SZ signal unchanged, this increase has to be balanced by a decrease of the gas density by a factor of two. It then affects our results in the following ways: (a) The infered total mass will be divided by a factor of two ($M_{gas}(r < 0.6\mathrm{Mpc}) = (0.61 \pm 0.04) \times 10^{14}\, h_{50}^{-5/2} \mathrm{M}_{\odot}$). The total mass will also increase by a factor of two and then be in agreement with the lensing measurements. (b) As far as we suggest an increase of the gas temperature balanced by a decrease of the gas density, the SZ signal will remain unchanged. On the opposite, the X-ray flux will decrease by more than a factor of 2 (scaling the X-ray flux as $n_e(0)^2 \sqrt{(T_g)}$). Consequently, the Hubble constant will be affect by a factor of 2 ($H_0 \propto F_{SZ}^2 / F_X$).

The previous scheme is very simple. The thermodynamic state of the intracluster medium is probably more complex mainly made of two gas components. A cold ($\propto$ 9keV), dense and peacked central component surrounded by a hot ($\propto$ 18keV), thin and extended component. In this case the cluster should present a non isothermal radial profile (assuming the spherical symmetry). This kind of hypothesis could explain the very strong degeneracy which we encountered while trying to determine the core radius (see Sec. 4.1). Unfortunately, the quality of our data is not good enough to argue in this direction. Nevertheless, this suggestion is not unlikely. Recent XMM-Newton observations have already shown such a behavior in other cooling flow clusters: A1795 (Arnaud et al. 2000; Tamura et al. 2001), A1835 (Peterson et al. 2000)

4.3. Point sources

The best fit model gives a flux of 5.7 ± 1.5mJy/beam for the central point source. This point source can be visualized on the data map after the subtraction of the SZ component. Figure 1d shows clearly an excess of positive emission in its center. The NVSS map (Condon et al. 1998) has been overplotted as contours. Both signals match very well in term of position.

This point source has already been observed at different frequencies. It has been detected in the NVSS by Condon et al. (1998) with a flux of 46.9 ± 1.9mJy at 1,4GHz. Komatsu et al. (1999) have reported various measurements of this point source: an OVRO flux of 10.1 ± 0.5 at 28.5GHZ, a NMA (Nobeyama Millimeter Array) flux of 5 ± 1.5mJy at 100GHz and a 2σ upper limit of 4.8mJy obtained with SCUBA at 350GHz. From this set of measurements and assuming a power law spectrum for the point source radio emission, they have derived: $F_{RS} = (55.7 \pm 1.0) \nu_{GHz}^{-0.47 \pm 0.02}$mJy. More recently, Komatsu et al. (2000) have observed it with the VLA at 8.46 and 22.46GHz. The respective detected flux are 22.42 ± 0.04 and 11.5 ± 0.17mJy.

Using those latest measurements, we update the point source power spectrum determination: $F_{RS} = (77.8 \pm 1.7)\nu_{GHz}^{-0.58\pm0.01}$ mJy. The quality of this fit is moderate, due to the very robust constraints given by some of the data points (see Fig. 4). It is difficult to conclude firmly that a single power spectrum can model correctly the synchrotron emission from radio wavelengths down to millimeter wavelengths. The intensity and the spectral shape of the synchrotron emission is driven by the internal magnetic field of the radio source. Furthermore its strength also drives the maximum frequency of emission allowed. To date, a lot of radio sources have been observed with various intensity and spectral shapes. Because of this high rate of variation from one source to an other and because of the lack of millimeter data, we are not able to state on an eventual cut-off in the spectral shape of our radio source. For this reason, we adopted the previously defined power law model. It provides us an estimation of the flux contributed by the central point source at 143GHz (2.1mm).

To explain the nature of the millimeter emission we have detected, we will now compare the residual radio flux expected at 143GHz (2.1mm) and 350GHz (850μm) from the previous power law spectrum to the flux respectively obtained from the DIABOLO data and from the SCUBA data. At 2.1mm, we have extrapolated: $F_{RS}^{est}(2.1\mathrm{mm}) = 4.3 \pm 0.3$mJy. This estimation is at 1σ compatible with our determination from the DIABOLO map. The 350GHz (eg: 805μm) flux can be estimated too: $F_{RS}^{est}(0.85\mathrm{mm}) = 2.7 \pm 0.4$mJy. Now, from the SCUBA data points published by Komatsu et al. (1999), we have subtracted the positive SZ contribution, computed from the cluster SZ spectrum and scaled by our y best fit value. The SZ radial profile has been obtained from the model C (see Sec. 4.1) convolved with the SCUBA beam (a Gaussian beam with σ_{FWHM} = 15"). We fixed the value of the signal offset (so-called DC offset) to 2.7mJy/beam as published by Komatsu et al. We finally deduced for the point source: $F_{RS}(0.85\mathrm{mm}) = 1.8 \pm 1.0$mJy. The low signal to noise ratio of this last flux does not allow us to consider this result as the detection of a real submillimeter point source.

Nevertheless, our DIABOLO flux and the SCUBA flux are both compatible with the estimation extrapolated from the point source power spectrum. For this reason, it seems reasonable to deduce that the point source emission seen in our map is likely due to the synchrotron millimeter tail of the central radio point source emission.

5. Conclusion

We have produced an extended map ($4'' \times 4''$) of the RXJ1347-1145 cluster with the DIABOLO photometer. We have drawn the distribution of the SZ signal up to 74" (0.6Mpc) from the cluster center. This SZ signal is as much extended as the X-ray emission and is the strongest SZ effect detected to date.

The SZ map allows us to directly derived the projected mass distribution and by the way to measure the cluster gas mass up to 0.6Mpc. We derived $M_{gas} = (1.1 \pm 0.1) \times 10^{14}\, h_{50}^{-5/2}\mathrm{M}_{\odot}$. The gas mass estimated within the same region, under the assumption of a classical β-model and the cluster parameters derived from the X-ray data, agrees with our value.

Due to the map noise level and to the observing strategy, we are not able to firmly conclude to the existence of substructure in the gas distribution. Nevertheless, our map presents some asymmetric features at more than a 2σ level.

At the moment, the first results of the Chandra and the XMM-Newton satellites, concerning the observation of galaxy clusters, already show some departure in the density distribution from the β-model symmetry, as well as in the temperature distribution from the isothermality (Fabian et al. 2000; Vikhlinin, Markevitch and Murray 2000; Arnaud et al. 2000; Tamura et al. 2001; Peterson et al. 2000). For this reason, the comparison of the upcoming Chandra and XMM-Newton X-ray obervations to the actual and the future SZ data (from interferometers and bolometer arrays) are needed to understand the cluster physical structure.

The authors want to thanks the IRAM staff (from astronomers to cookers). Thanks to N. Aghanim, E. Komatsu, M. Hattori and Y. Suto for their fruitful comments and discussions. We are very grateful to the anonymous referee for the quality of his report that helped us to improved and clarify our paper. DIABOLO is supported by the Programme National de Cosmologie, Institut National pour les Sciences de l'Univers, Ministère de l'Education Nationale de l'Enseignement Supérieur et de la Recherche, CESR, CRTBT, IAS-Orsay and LAOG.

REFERENCES

Allen, S.W., 1998, MNRAS, 296, 392

Arnaud, M. et al., *A&A*(special Letter issue on XMM), astro-ph/0011086

Benoit A. et al. 2000, *Astron. Astrophys. Suppl.*, 141, 523

Bahcall, N. A. and Fan, X. 1998, ApJ, 504, 1

Birkinshaw, M. 1999, Phys. Rep., 310, 97

Carlstrom, J. E., Joy, M. K., Grego, L., Holder, G. P., Holzapfel, W. L., Mohr, J. J., Patel, S. and Reese, E. D. 2000, Physica Scripta Volume T, 85, 148

Cavaliere, A. and Fusco-Femiano, R. 1976, A&A, 49, 137

Condon, J. J., Cotton, W. D., Greisen, E. W., Yin, Q. F., Perley, R. A., Taylor, G. B. and Broderick, J. J. 1998, *Astron. J.*, 115, 1693

Désert, F.X., et al. 1998, New Astronomy, 3, 655

Fabian A.C. et al. 2000, accepted by MNRAS, astro-ph/0007456

Fischer, P. and Tyson, J. A. 1997, *Astron. J.*, 114, 14

Jones, M. et al. 1993, Nature, 365, 320

Komatsu, E., Kitayama, T., Suto, Y., Hattori, M., Kawabe, R., Matsuo, H., Schindler, S. and Yoshikawa, K. 1999, *ApJ (Lett.)*, 516, L1

Komatsu, E., Matsuo, H., Kitayama, T., Hattori, M., Kawabe, R., Kohno, K., Kuno, N., Schindler, S., Suto, Y. and Yoshikawa, K. 2000, *PASJ*, submitted

Oukbir, J., Bartlett, J. G. and Blanchard, A. 1997, A&A, 320, 365

Peterson, J. R. et al., *A&A*(special Letter issue on XMM), astro-ph/0010658

Pointecouteau, E., Giard, M. and Barret, D. 1998, A&A, 336, 44

Pointecouteau, E., Giard, M., Benoit, A., Désert, F. X., Aghanim, N., Coron, N., Lamarre, J. M. and Delabrouille, J. 1999, *ApJ (Lett.)*, 519, L115

Sadat, R., Blanchard, A. and Oukbir, J. 1998, A&A, 329, 21

Sahu, K. C. et al. 1998, *ApJ (Lett.)*, 492, L125

Schindler, S. et al. 1995, A&A, 299, L9

Schindler, S., Hattori, M., Neumann, D. M. and Boehringer, H. 1997, A&A, 317, 646

Sunyaev, R. and Zel'dovich, Y. 1972, Comments Astrophys. Space Phys., 4, 173

Tamura, T. et al. 2001, *A&A*Letters , astro-ph/0010362

Vikhlinin A., Markevitch M. and Murray S.S., submitted to ApJ, astro-ph/0008496

This 2-column preprint was prepared with the AAS LaTeX macros v5.0.

Fig. 1.— (a) 2.1mm map of RXJ1347-1145 obtained with the DIABOLO photometer. This map and the three others have been smoothed by a gaussian filter with 20" FWHM. The 1σ noise level in term of flux is 1mJy in a pixel of $10'' \times 10''$ (equivalent to 0.5mJy/beam in the 22' DIABOLO beam and to 0.3mJy/beam in the 30" FWHM effective beam after smoothing). (b) Residual map after subtraction of the best fit model (SZ plus point source, see text). In the maps *a* and *b* the overlying contours correspond to the 1, 2, 3, 4 and 5 σ detection levels. The negative and positive contours are respectively drawn with solid and dashed lines. (c) RXJ1347-1145 SZ signal (after subtraction of the point source best fit model) compared to the X-ray cluster emission. The different contours overplotted correspond to 3, 5, 10, 30, 50, 70 and 90% of the X-ray maximum of emission. (d) Point source detection at 2.1mm after subtraction of the SZ best fit model. The contours overlying correspond to the NVSS map (1, 10, 30, 50, 70 and 90% of the radio maximum emission). The central position in the four map correspond to the position of the X-ray center: $\alpha_{2000} = 13^{\rm h}47^{\rm m}31^{\rm s}$, $\delta_{2000} = -11°45'11"$.

Fig. 2.— RXJ1347-1145 radial profile at 2.1mm computed from the DIABOLO 2.1mm map. The data point are plotted with their associated 1σ error bars. The best fit model (including an SZ component and a point source component, see text) is overplotted (solid line). The residual radial profile is plotted as a dashed line.

Fig. 3.— RXJ1347-1145 gas mass profile computed directly from the 2.1mm map. The solid line represents the gas mass profile of the SZ best fit model. The integral of the DIABOLO beam (dashed line) has been overplotted and scalled to the gas mass profile to show the extension of the SZ signal.

Fig. 4.— Central point source spectum from 1.4 to 350GHz.

Table 1: Best fit parameters.

Models	$y(0)$ $[10^{-4}]$	θ_c (arcsec)	β	F_{RS} (mJy)	$\chi^2/(n-1)^{\mathrm{a}}$
A	$4.1^{+1.7}_{-0.4}$	$56.3^{+12.0}_{-19.1}$	$0.89^{+0.26}_{-0.61}$	0^{b}	1.1
B	$5.3^{+0.8}_{-0.3}$	$32.4^{+18.4}_{-21.5}$	0.56^{b}	0^{b}	0.9
C	$5.7^{+0.3}_{-1.6}$	$12.4^{+40.2}_{-12.4}$	$0.51^{+0.34}_{-0.11}$	$3.4^{+2.6}_{-3.7}$	1.1
D	$5.7^{+0.4}_{-0.6}$	$14.8^{+28.7}_{-4.7}$	0.56^{b}	$4.1^{+39.3}_{-5.9}$	0.9
E	$7.9^{+0.4}_{-0.5}$	8.4^{b}	0.56^{b}	$5.7^{+1.4}_{-1.6}$	1.1

[a] where (n-1) is the number of degrees of freedom

[b] fixed parameter, see text

Table 2: Fluxes in $50'' \times 50''$ SE, NE, NW and SW regions as defined by Komatsu et al. (2000). The column respectively gather the DIABOLO fluxes (1), the residual flux after the subtraction of the best fit model (2), the NOBA/NRO fluxes (3). Columns (1) and (3) have to be compared. The second column try to highlight some eventual excess (positive or negative). For each collumn the associated 1σ noise flux is quoted.

Regions	map (mJy)	residual map (mJy)	NOBA/NRO (mJy)
SE	-12.2	-0.8	-11.3
NE	-9.9	-0.7	-4.7
NW	-10.1	-0.4	-3.3
SW	-6.8	2.8	-6.1
1σ noise	1.4	1.4	2.0

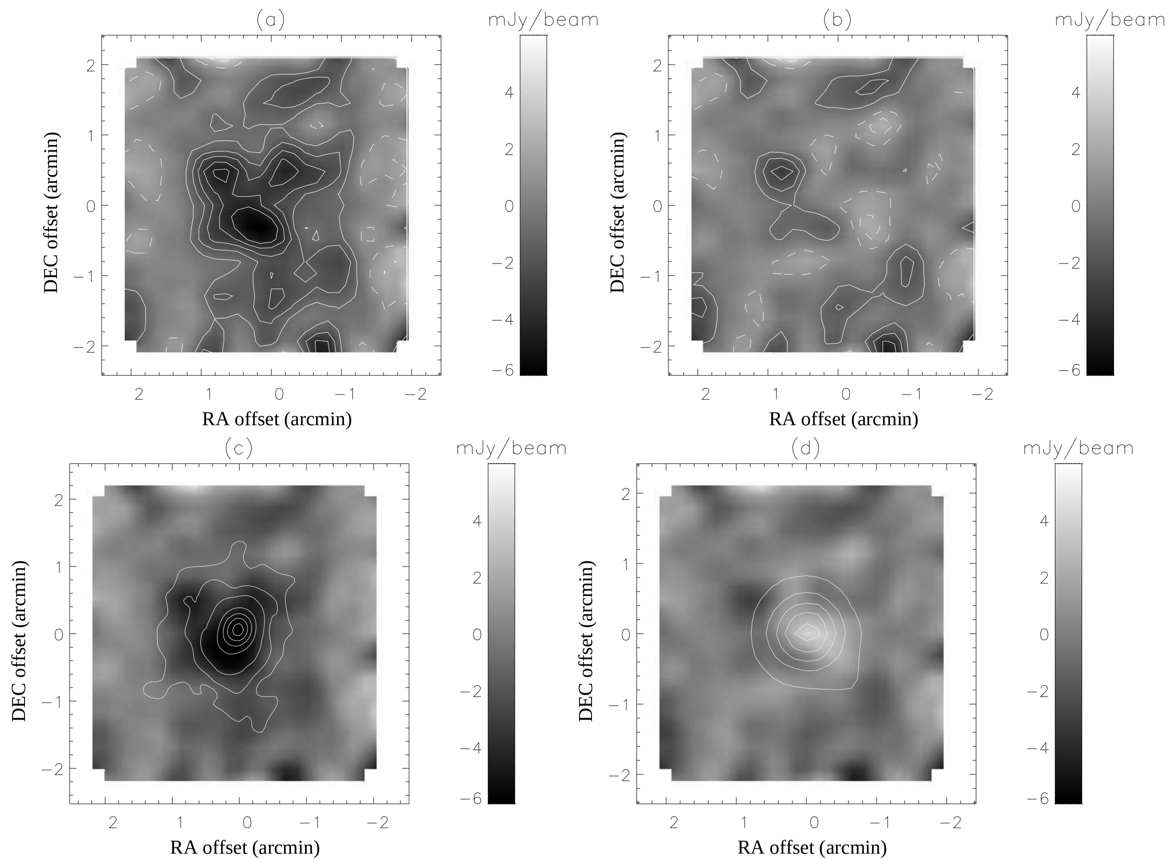
(a)
(b)
(c)
(d)
mJy/beam
DEC offset (arcmin)
RA offset (arcmin)

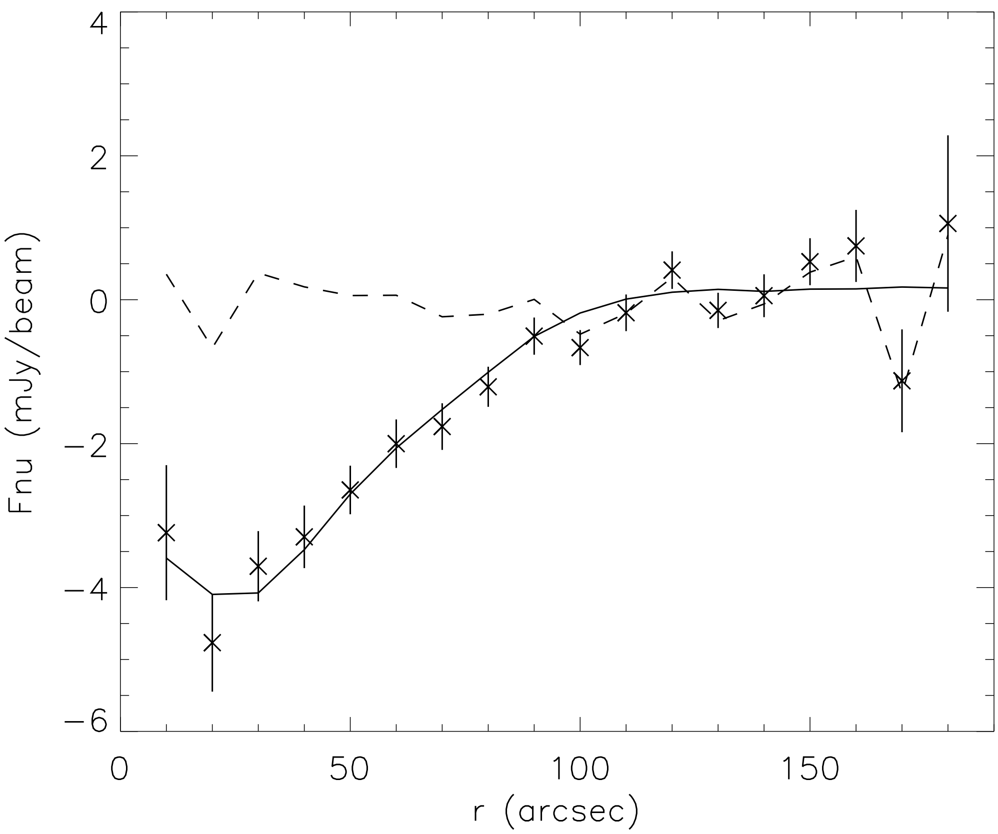

4
2
0
−2
−4
−6
Fnu (mJy/beam)
0
50
100
150
r (arcsec)

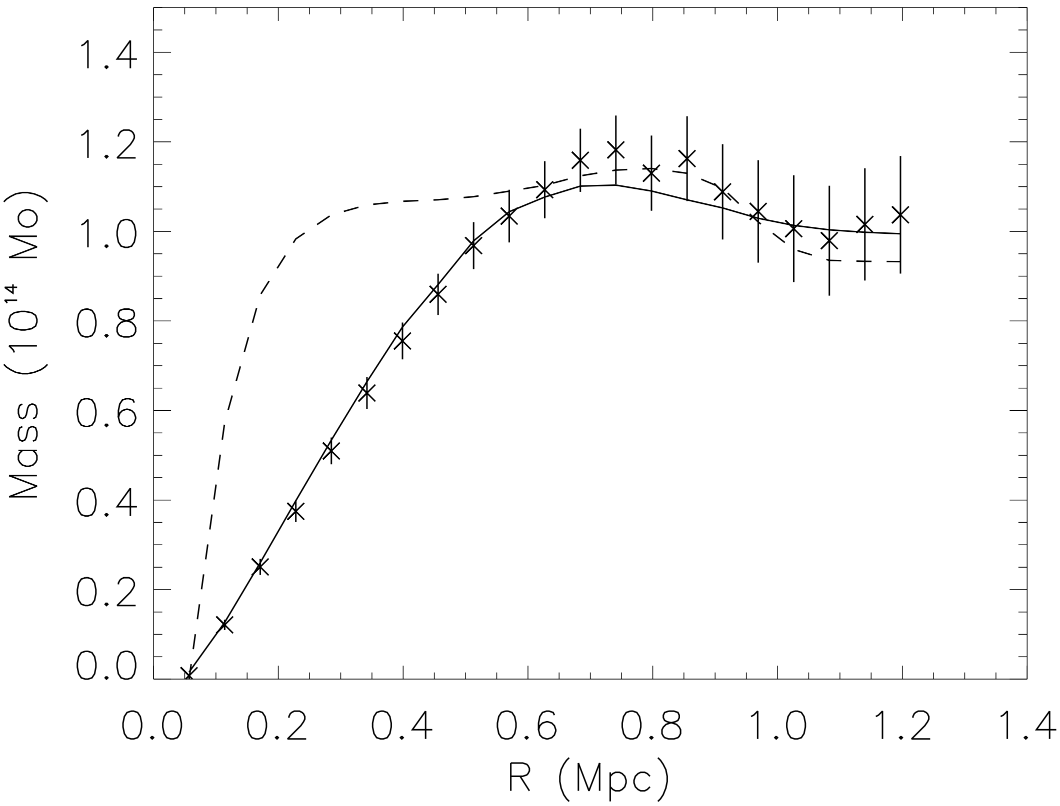
Mass (10¹⁴ Mo)
R (Mpc)
0.0
0.2
0.4
0.6
0.8
1.0
1.2
1.4

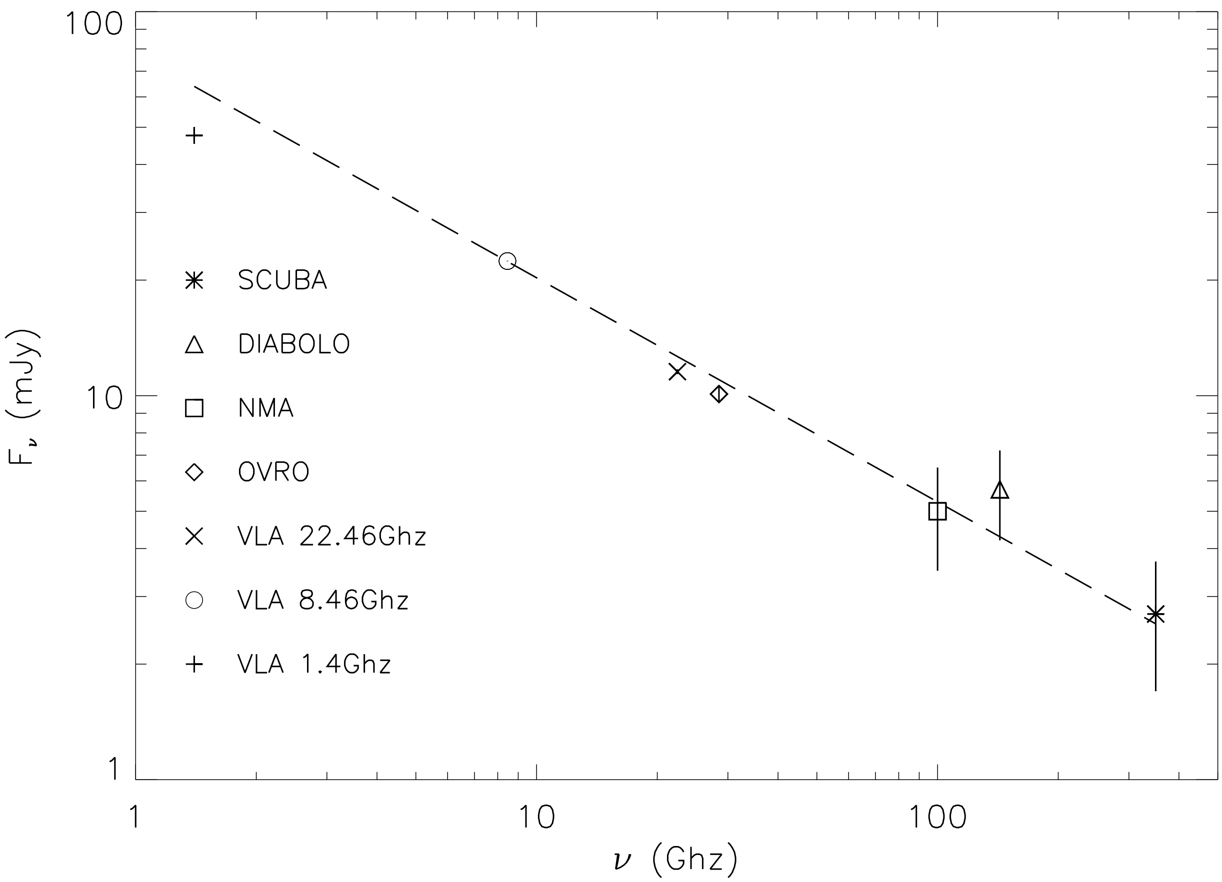

100
10
1
1
10
100
F_ν (mJy)
ν (Ghz)
SCUBA
DIABOLO
NMA
OVRO
VLA 22.46Ghz
VLA 8.46Ghz
VLA 1.4Ghz